Nanobactericides Derived from Cinnamon Bark Extract: Phytochemical Profiling and Antibacterial Efficacy Against Bacterial Panicle Blight in Rice

Qamar Mohammed Naji[1,2,*], Dzarifah Mohamed Zulperi[3,*] , Khairulmazmi Ahmad [4,] Erneeza Mohd Hata[5]

[1] Department of Plant Protection, Faculty of Agriculture, Universiti Putra Malaysia, Serdang 43400, Malaysia.

[2] Directorate of the planting of holy Karbala, Iraqi Ministry of Agriculture.

[3] Head of department of Plant Protection, Faculty of Agriculture, Universiti Putra Malaysia, Serdang 43400, Malaysia.

[4] Institute of Tropical Agriculture and Food Security (ITAFoS), Universiti PutraMalaysia, Serdang 43400,Malaysia

[5] Institute of Plantation Studies (ikp), Universiti PutraMalaysia, Serdang 43400,Malaysia

*Correspondence: dzarifah@upm.edu.my (D.M.Z)

Running title: Activity and Nanobactericides of CBE

ABSTRACT

Bacterial panicle blight (BPB), caused by the Gram-negative aerobic bacterium *Burkholderia glumae (B.glumae)*, poses a significant threat to global rice production. Cinnamon bark extract (CBE) has demonstrated potent antioxidant and antimicrobial properties due to its high concentration of bioactive compounds, including eugenol and cinnamaldehyde. To enhance the efficacy and stability of these volatile compounds, this study employed nanotechnology and encapsulation techniques. The objective was to develop a CBE-based nanoformulation to inhibit *B. glumae* and control BPB in rice. CBE-chitosan (CBE-CS) nanoformulations were synthesized using ionic cross-linking between chitosan and trisodium phosphate (TPP) at various concentrations (0%, 0.5%, 1%, 2%, and 4% TPP). More than 15 active compounds were identified in CBE, including (Z)-3-Phenylacrylaldehyde, 2-Propenoic acid, 3-(2-hydroxyphenyl), cinnamaldehyde dimethyl acetal, and hexadecanoic acid. Bacterial membrane damage was significantly greater in treatments with CBE compared to untreated controls. The synthesized nanoparticles ranged in size from 43.66 nm to 106.1 nm, with encapsulation efficiencies between 48.65% and 48.78%, and loading capacities between 25.65% and 33.9%. Scanning electron microscopy (SEM) revealed spherical and homogeneous nanoparticles, while FTIR and XRD analysis confirmed the successful encapsulation of CBE in the chitosan nanoparticles. The antibacterial activity of the nanoformulations showed inhibition zones ranging from 7.5 to 11.8 mm, with the CBE-CS formulation containing 0.5% TPP demonstrating the highest efficacy (MIC = 15.6 μmol/ml; MBC = 31.25 μmol/ml).

Keywords: Bacterial panicle blight, *Burkholderia glumae*, Cinnamon bark extract, nanoformulation, Rice.

1. **Introduction**

Since the dawn of civilization, archaeological evidence suggests that rice (*Oryza sativa*) has been a fundamental food source for humans, with its cultivation dating back to 1500-1000 BC (Verma & Srivastav, 2020). Today, rice remains a staple food for approximately 40% of the global population, particularly in the least developed countries (Zhang et al., 2022). The optimal climatic conditions for rice cultivation, including high humidity and abundant water, are prevalent in many Asian countries, especially in tropical regions (Rashid et al., 2022). In Malaysia, rice is the third most important crop after rubber and oil palm, with the states of Kedah and Perlis being key centers of rice production. However, rice fields are highly susceptible to a variety of diseases caused by microbes, fungi, and bacteria, which can severely affect productivity. Over 70 different diseases have been identified as impacting rice fields, with five to six major bacterial diseases attacking various parts of the rice plant, including the seedlings, leaves, leaf sheath, grains, stem, and roots (Faizal Azizi & Lau, 2022). One of the most severe bacterial diseases affecting rice worldwide, including in Peninsular Malaysia, is bacterial panicle blight (BPB), caused by *Burkholderia glumae* (*B. glumae*) (Ramachandran et al., 2021). This pathogen can cause up to a 75% yield loss and significantly reduce the quality of the affected plants, presenting a major challenge to rice cultivation. *B. glumae* thrives at optimal temperatures around 30°C, though it can survive in temperatures as high as 41°C. The bacteria infect seeds, enter plumules through stomata and wounds, and proliferate in the intercellular spaces of parenchyma during seed germination. This growth leads to the production of toxic substances like toxoflavin, which results in rice seedling rot (Rahman et al., 2024). Several strategies have been employed to manage BPB in rice cultivation (Chompa et al., 2022). Biological control methods, such as using harmless *Burkholderia* isolates, have been effective in reducing bacterial toxins and curbing rice grain rot.

Cultural practices, including the use of pathogen-free seeds, also help limit bacterial transmission (Kumar et al., 2023). While chemical treatments like oxolinic acid have been used to control seedling and inflorescence rot (Han et al., 2021), the rise of resistant *B. glumae* strains and the negative residual effects of chemicals on soil and plants have decreased their use. Recently, natural plant extracts such as cinnamon bark have emerged as promising antibacterial agents for BPB control (Sharifi-Rad et al., 2021). Cinnamon, a widely used spice, is derived from the inner bark of trees belonging to the genus *Cinnamomum* (Farooq et al., 2023). Both the bark and leaves are used in cooking and in various natural medicinal applications. Cinnamon bark extract (CBE) is rich in bioactive compounds such as eugenol, cinnamaldehyde, cinnamic acid, and coumarin (Mini Raj et al., 2023). These components exhibit diverse pharmacological properties, including antifungal, antibacterial, anti-inflammatory, antioxidant, antidiabetic, nematocidal, insecticidal, and anticancer effects (Anuranj et al., 2022).

With significant advancements in plant disease control and the advent of nanotechnology, organic nanoparticles (ONPs) and nanostructures have emerged as a promising field for managing plant diseases (Koul et al., 2021). While many methods exist for synthesizing inorganic nanoparticles from metals like gold and silver or semiconductors such as Si, ZnO, Ge, and GaAs, fewer techniques are available for producing ONPs. Organic nanomaterials have gained attention due to their unique structural and optical properties, which differ from their bulk forms. One of the most promising polymers for delivering agrochemicals and micronutrients in nanoparticles is chitosan (CS) (Mujtaba et al., 2020). Chitosan is a natural amino polysaccharide derived from fungal cell walls, the exoskeletons of insects and crustaceans, and other natural sources. Commercially, CS is produced by partially de-N-acetylating chitin. It is considered more effective than chitin due to its higher content of chelating amino groups and greater chemical modifiability.

As a cationic polyelectrolyte, chitosan exhibits unique properties, including its abundance, biocompatibility, biodegradability, and nontoxicity (Ul-Islam et al., 2024). Additionally, CS nanoparticles (NPs) offer great potential as nanocarriers, capable of encapsulating both hydrophilic and hydrophobic compounds (Pathak et al., 2023). In this study introduces CBE as a novel natural antibacterial ingredient against *B. glumae*. Compared to synthetic bactericides, the CBE nanoparticle formulation offers a superior strategy for combating plant pathogen infections in rice crops. The primary objective of this study is to develop a chitosan-loaded CBE nanoparticle formulation that effectively inhibits the growth of *B. glumae* in rice plants.

2. Materials and method

2.1. Raw materials

Chitosan (molecular weight 200 kDa, with a deacetylation degree of ≥75%) was procured for the study. Cinnamon bark (*Cinnamomum cassia*) was sourced from local markets in Malaysia. The raw materials were carefully transported to the laboratories of the Department of Plant Protection, Faculty of Agriculture, Universiti Putra Malaysia UPM, where they were utilized for experimental procedures and subsequent evaluation of results.

2.2 Extraction of Cinnamon Bark Extract

Cinnamon (Cinnamomum cassia) bark was obtained from market, wash, dry and ground into a fine powder using a blender. The powdered cinnamon (20 g) was then macerated in 200 mL of methanol (70% v/v) in a tightly sealed container for 48 hours at room temperature with intermittent shaking. After maceration, the cinnamon-methanol mixture was filtered through Whatman filter

110   paper (Grade 1). The filtrate was concentrated under reduced pressure using a rotary evaporator at

111   40°C to remove the methanol and obtain the concentrated cinnamon extract.

112   2.3 Determination of the phytochemical compounds

113   A gas chromatography/mass spectrometry (GC-MS) analysis was performed to evaluate the

114   volatile compounds and their abundances in CBE. This investigation using a Shimadzu QP-2010

115   Ultra GC-MS system as described by Wang et al. in (Wang et al., 2020). The system features a

116   gas chromatograph connected to a mass spectrometer and utilizes an SLB-5ms capillary column

117   (30 m length x 0.25 mm ID x 0.25 µm film thickness). The oven temperature program began at

118   50°C, then increased by 10°C per minute to 250°C, and finally increased to 300°C. The analysis

119   was conducted at 70 eV, with a scan interval of 0.1 seconds, recording fragments ranging from 40

120   to 700 Da.

121   2.4. Preparation of cinnamon bark extract-loaded chitosan submicron
122   emulsions

123   A nanobacterial bactericide targeting *B. glumae* was prepared using chitosan loaded with CBE,

124   following the method described by (Maluin et al., 2019) with necessary modifications. The CBE

125   was incorporated into chitosan nanoparticles using ionic gelation technique. Chitosan powder,

126   sourced from Sigma Aldrich (low molecular weight, ≥ 75% deacetylation), was dispersed in a

127   diluted acetic acid solution at a 1% (v/v) ratio and continuously stirred overnight at room

128   temperature to form a 1% (w/v) CS solution. Subsequently, the CBE was mixed with Tween 80

129   (HLB 15.9) in a 1:1 (v/v) ratio, creating a CBE-Tween 80 mixture. This was stirred continuously

130   for 1 hour at room temperature until a homogeneous solution was achieved. To initiate cross-

131   linking, a modified ionic gelation method was employed. A 5 ml portion of the 1% CS solution

132   was combined with the CBE-Tween 80 mixture under continuous stirring until the mixture became

133   viscous. TPP solutions at concentrations of 0%, 0.5%, 1%, 2%, and 4% (w/v) were then added to

134   15 ml of the CS mixture, stirred at 1000 rpm for 15 minutes at room temperature. Finally, 5 ml of

135   distilled water was added under magnetic stirring at room temperature and left for 24 hours to

136   complete the formulation. The resulting nanobactericidal formulation was designated CBE-CS.

137   Fig. 1 illustrates the preparation process of CBE-CS.

138   **Fig. 1: Preparation of chitosan nanoparticles loaded with cinnamon bark extract using ionic**

139   **gelation method**

140   ## 2.5. Characterization of emulsions

141   **2.5.1. Particle size, polydispersity index and zeta potential**

142   The mean particle size (PS), polydispersity index (PDI), and zeta potential (ZP) of CBE-CS

143   nanoparticles were evaluated using a Zetasizer Nano ZS90 (Malvern, UK) through dynamic light

144   scattering (DLS) at 25°C (Lunardi et al., 2021). Zeta potential, determined from electrophoretic

145   mobility using the Helmholtz–Smoluchowski equation under a 40 V/cm electric field, assessed

146   nanoparticle stability by indicating potential variation between the dispersion medium and the

147   stationary fluid layer (Ağardan, 2020). Morphology was examined via SEM after coating the

148   samples with a thin carbon layer. Stability was tested by storing various formulations at room

149   temperature. All measurements, conducted in triplicate (n = 3), utilized water's viscosity, refractive

150   index, and absorption parameters provided by the Malvern software

151   **2.5.2. Transmission electron microscopy (TEM)**

152   High-resolution TEM was employed to investigate the morphology of CBE-CS nanoparticles,

153   with modifications to the method described by (Alghuthaymi et al., 2021). The samples were first

154   diluted with distilled water and then deposited onto 200-mesh Formvar-coated copper grids for

155   TEM imaging. The grids were subjected to low pressure and allowed to dry overnight at room

156   temperature. The nanoparticles were observed under TEM without any staining.

157   **2.5.3. Fourier transform infrared spectroscopy (FTIR)**

158   To analyze the active compounds in the CBE-CS nano extract, Fourier Transform Infrared

159   (FTIR) spectroscopy was employed. This technique was utilized to identify the various chemical

160   bonds within the molecules by generating an IR absorption spectrum (Veerasingam et al., 2021).

161   The materials analyzed included powdered chitosan and TPP, along with four liquid samples of

162   the CBE-CS nano extract and one sample of a simple CBE formulation for comparison.

163   **2.5.4. Encapsulation efficiency and loading capacity**

164   Encapsulation efficiency (EE) and loading capacity (LC) of CB-CS nanobactericide formulations

165   were evaluated using UV-Vis spectrophotometry with slight modifications to a standard protocol

166   (Hoang et al., 2022). Freeze-dried nanobactericide (400 mg) was mixed with 5 mL of 1 M HCl,

167   vortexed, and combined with 2 mL of ethanol, then incubated at 60°C for 12 hours. After

168   centrifugation at 6000 rpm for 10 minutes at 25°C, the supernatant was analyzed with a UV-Vis

169   spectrophotometer (200–400 nm). A calibration curve (R^2 = 0.9859) was used to quantify CBE.

170   Triplicate measurements ensured accuracy, and EE and LC were calculated using standard

171   formulas (Hoang et al., 2022).

172
$$EE\,\% = \frac{weight\ of\ CBE\ in\ the\ nanoparticles}{The\ initial\ weight\ of\ CBE\ in\ the\ system} \times 100 \qquad (1)$$

$$LC \% = \frac{weight\ of\ CBE\ in\ the\ nanoparticles}{weight\ of\ nanoparticles} \times 100 \qquad (2)$$

2.5.5. Invitro release of nanobactericde formulation

The release analysis of the CBE-CS nanopesticide formulation was performed using a modified method from (Kaboudi et al., 2023). A 300 µL sample of the formulation was dissolved in 30 mL of phosphate-buffered saline (PBS, pH 7.4) at room temperature. At specific intervals, 3 mL samples were collected for analysis, replacing the same volume with fresh PBS to maintain consistency. The released CBE concentration was measured using UV-Vis spectroscopy, and the total release was calculated using formula (3).

$$Release\ (\%) = \sum_{t=0} \frac{M_t}{M_i} \times 100 \qquad (3)$$

where M_t represents the cumulative amount of CBE collected at time t, and M_i is the initial weight of CBE incorporated into the formulation. This formula provides the percentage of CBE released over time, reflecting the release kinetics and efficiency of the nanopesticide formulation.

2.5.6. Evaluation of the antibacterial activity of CBE-CS

The antibacterial efficacy of the nano-CBE-CS formulation against *B. glumae* was evaluated using disk diffusion assays. A *B. glumae* suspension (10^8 CFU/mL) was prepared in sterile distilled water and spread evenly on Mueller-Hinton Agar (MHA) plates. Sterile Whatman filter paper discs (6 mm diameter) were impregnated with 20 µL of formulations (CBE-CS 0, 0.5, 1, 2, and 4) in a laminar flow hood, with streptomycin (15 µg/mL) and distilled water serving as positive and negative controls, respectively. The discs were placed on the inoculated plates, left at room temperature for 30 minutes for diffusion, and incubated at 37°C for 24 hours. Inhibition zones

194 were measured in millimeters, and bacterial inhibition percentages were calculated using formula

195 (4). Each experiment was performed in triplicate and repeated twice (Chavez-Esquivel et al.,

196 2021).

197 $$Inhibition\ effect\ (\%) = \frac{iextract\ inibition\ hold\ diameter\ (mm)}{inhibition\ zone\ of\ positive\ control\ (mm)} \times 100 \qquad (4)$$

198 MEC and MBC tests were performed by double dilution method on the CBE-CS

199 nanobactericidal formulation at a concentration of 0.5% TPP due to the small diameter of the

200 nanoparticles and the high zeta potential value of this concentration.

201 **2.5.7 Time killing analysis**

202 To evaluate the bactericidal effects of the CBE-CS nanocide formulation, a growth curve

203 analysis was conducted. In this study, a 96-well microplate was used to assess the bactericidal

204 activity of the CBE-CS nanocide formulation. Each well was first filled with 150 μL of Mueller-

205 Hinton Broth (MHB), followed by the addition of 150 μL of the CBE-CS nanocide formulation at

206 concentrations corresponding to 0.5 MIC, 1 MIC, and 2 MIC. A control well received only 1%

207 Tween 80. Subsequently, 50 μL of *B. glumae* suspension (10^7 CFU/mL) was added to each well.

208 The microplate was incubated at 37°C, and the optical density (OD) at 600 nm of the liquid culture

209 was measured at regular intervals using a spectrophotometer to monitor bacterial growth (Cava-

210 Roda et al., 2021)

211 # 3. Results and discussion

212 ## 3.1. Determination of phytochemical constituents

213 The qualitative and quantitative analysis of CBE was conducted using GC-MS. Detailed on the

214 various bioactive compounds found in CBE is presented in Table 1.

Table 1: Phytochemical constituents in CBE identified by GC-MS, comparing Retention

Times (Rt), Retention Index (RI), Area %, molecular formula, mass spectral (MS), and

Height Data with databases FFNSC1.3.lib, NIST11.lib, and WILEY229.lib.

No.	Chemical Component	Rt (min)	RI	Area (%)	Formula	MS	Height%
1	Cinnamaldehyde	21.165	1218	0.58	C9H8O	373	1.08
2	(Z)-3-Phenylacrylaldehyde	23.707	1189	51.24	C9H8O	295	37.12
3	Guaiacol	25.582	1309	0.79	C9 H10 O2	332	1.23
4	Eugenol	27.587	1392	3.13	C10H12O2	398	5.14
5	Coumarin	28.723	1386	1.12	C9 H8 O2	335	1.61
6	Cinnamaldehyde dimethyl acetal	29.477	1287	11.23	C11H14O2	361	16.77
7	2-Propenoic acid, 3-(2-hydroxyphenyl)	31.160	1577	13.24	C9H8O3	343	14.15
8	Muurolene	33.938	1497	1.10	C15 H24	404	1.60
9	Eugenyl acetate	34.917	1521	2.18	C12 H14 O$_3$	388	3.21
10	2-Propenal, 3-(2-methoxyphenyl)-	35.063	1378	2.99	C10H10O$_2$	363	4.31
11	1,3-Benzenediol, 4-propyl	37.942	1434	1.95	C9H12O2	367	2.20

12	Hexadecanoic acid	51.155	1977	5.48	C16	H32	397	5.85
					O2			
13	9-Octadecenoic acid (Z)-, methyl ester	55.625	2085	0.68	C19H36O2		383	1.08
14	10(E),12(Z)-Conjugated linoleic acid	56.660	2183	2.06	C18H32O2		371	2.06
15	Oleic Acid	56.845	2175	2.23	C18H34O2		383	2.61

218

219 The identification of constituents in CBE was performed by comparing their retention times and

220 retention indexes with data from libraries such as FFNSC1.3.lib, NIST11.lib, and WILEY229. The

221 gas chromatography analysis of CBE revealed the presence of 15 active substances. Among these

222 compounds, (Z)-3-Phenylacrylaldehyde was found to be the most predominant, constituting

223 51.24% of the total composition. Following this, 2-Propenoic acid, 3-(2-hydroxyphenyl)

224 accounted for 13.24%, while Cinnamaldehyde dimethyl acetal and Hexadecanoic acid were

225 present at concentrations of 11.23% and 5.48% respectively. Additionally, 2-Propenal, 3-(2-

226 methoxyphenyl) was identified at 3.99%, followed by Eugenol (3.13%), Oleic Acid (2.23%), and

227 Eugenyl acetate (2.18%). Furthermore, 10(E),12(Z)-Conjugated linoleic acid was detected at

228 2.06%. The analysis also revealed the presence of 4 aldehydes within the CBE. Apart from the

229 compounds, the remaining constituents were found in smaller quantities, each comprising less than

230 2% of the specimen. Specifically, 1,3-Benzenediol, 4-propyl was identified at 1.95%, followed by

231 Coumarin (1.12%), Muurolene (1.10%), and Guaiacol (0.79%). Additionally, 9-Octadecenoic acid

232 (Z)-, methyl ester and Cinnamaldehyde were detected at concentrations of 0.68% and 0.58%

233 respectively. Fig. 2 illustrates the chemical analysis and characterization of CBE conducted using

234 GC-MS, highlighting the identification of its key compounds.

235 **Fig.2: GC-MS chromatogram of CBE, depicting phytochemical analysis characterization of**

236 **CBE**

237

238 3.2. Size, polydispersity index and zeta potential

239 The physical properties of nanomaterials such as PZ, PDI, and ZP contribute to determining

240 their behavior pattern within different biological environments. The size distribution was measured

241 in a Zeta sizer Pro (Malvern Instruments Ltd, UK) and the results obtained represent the average

242 value of three samples. While the zeta potential was measured in triplicate for the dispersed

243 nanoparticles of each nanoparticle suspension using a Zeta sizer Pro with a DTS1070 zeta cell

244 (Malvern Instruments Ltd, UK). From the results presented in Table 2, it is evident that the

245 concentration of TPP plays a crucial role in determining the average hydrodynamic diameter of

246 the particles in the CBE-CS.

247 **Table 2: The impact of TPP concentration on the CBE-CS nanobactericide formulation's**

248 **average PS, PDI, and ZP**

Nano bactericide	Average size (d. nm)	PDI	Zeta Potential (mV)	Mob μmcm/Vs	Cond mS/cm
0% TPP	435.68±22.14a	1.00±0.00a	7.79±0.04a	-0.47±0.04d	0.97±0.02a

0.5% TPP	43.66±0.23a	0.28±0.03 c	1.78±0.04b	0.61±0.03a	0.34±0.02c
1% TPP	51.72±0.04a	0.57±0.02 b	1.01±0.01b	-0.20±0.06c	0.90±0.03a
2% TPP	79.67±0.17a	0.68±0.01 b	-2.58±0.08c	0.13±0.03b	0.53±0.07b
4% TPP	106.06±0.42 a	0.96±0.00 a	-6.11±0.61d	0.07±0.01b	0.90±0.02a
Mean 1-30	1.08E+04	0.661	0.396	0.03099	0.732
Std Dev	1.96E+04	0.325	4.81	0.3767	0.258

249

At 0% TPP, the particles exhibited a relatively large average size of 790.5 d.nm with a PDI index of 1, indicating significant polydispersity and potential instability in the formulation. As the TPP concentration was increased to 0.5%, there was a dramatic reduction in particle size to 43.66 d.nm, accompanied by a more uniform distribution, as reflected by a lower PDI of 0.288. This initial decrease in size suggests that TPP may facilitate the formation of more stable, smaller nanoparticles by promoting cross-linking within the extract. However, as the TPP concentration increased further, the average particle size began to rise, with measurements of 51.72 d.nm (PDI 0.481) at 1% TPP, 79.82 d.nm (PDI 0.576) at 2% TPP, and 106.1 d.nm (PDI 0.96) at 4% TPP. This trend of increasing particle size with higher TPP concentrations indicates a shift towards agglomeration, likely due to excessive cross-linking or the potential leakage of TPP onto the particle surfaces, which promotes sedimentation and aggregation. The increasing PDI values with

261 higher TPP concentrations further support the notion of growing heterogeneity within the particle

262 population (Somenath Das et al., 2020) and (Hasheminejad et al., 2019).

263 Consistent with earlier research, particularly studies by Huang et al. in (Huang et al., 2009)

264 and Calvo et al. in (Calvo et al., 1997). it was found that PDI values below 0.45 correspond to a

265 narrow size distribution, like what was observed at 0.5% TPP in the current study. These previous

266 studies demonstrated that the cross-linking of chitosan with TPP resulted in the formation of

267 submicron particles with PDI values less than 1, which aligns with the findings of this

268 investigation. In this study, the positive ZP values observed indicate a higher concentration of

269 hydrogen ions (H+) relative to hydroxyl ions (OH−) around the particle surfaces. This

270 phenomenon is typically attributed to the protonation of amino groups (NH3+) present in chitosan

271 (Prasad et al., 2022). The observed decrease in zeta potential values with increasing TPP

272 concentrations suggests a reduction in positive peripheral charges. This is likely due to the

273 interaction of TPP with the particle surface, which diminishes the number of protonated amino

274 groups (NH3+) on the chitosan particles (Fernández-Díaz et al., 2017). The study findings align

275 with previous reports indicating that for an emulsion to remain physically stable, an electrical

276 potential close to ±30 mV is required. Notably, all concentrations of the nano extract tested in the

277 current experiment achieved this stability threshold. These results corroborate the findings of

278 earlier studies, including those by (Deshi et al., 2024), which also reported similar behaviors in

279 systems involving chitosan and zeta potential measurements.

3.3. Transmission electron microscopy (TEM)

281 The TEM images in Fig. 3 (A) revealed that the nanocomposite was nearly circular when TPP

282 was absent. In contrast, Fig.3 (B to D) demonstrated that the average size of the nanocomposite

283   increased to 31 nm, 60 nm, and 73 nm for CBE-CS 0.5, CBE-CS 1, and CBE-CS 2, respectively,

284   with a sharp and distinctly crystalline surface. The results also indicated that particle size increased

285   with rising TPP concentration, as observed in the TEM images. The spherical nanoparticles

286   exhibited lighter edges than their centers, suggesting TPP coating. Despite some particle

287   clustering, the overall composition displayed a homogeneous distribution of the extract, with a

288   distinctly crystalline nanoparticle surface.

289   **Fig.3: TEM images of CBE-CS nanobactericide formulation with different concentrations**

290   **of TPP: (A) 0%, (B) 0.5 % (C) 1%, (D) 2% and (E) 4% (scale bar is 200 nm)**

291

292   3.4 Morphology and FTIR spectroscopy of emulsions

293   The results of FTIR spectroscopy analysis used to determine the chemical composition of the

294   samples are shown in Fig.4. The characteristic values of pure chitosan indicate the presence of

295   many active chemical compounds, as the peak at 3556 cm-1 indicates the presence of O-H alcohol

296   stretching, the peak at 3329 cm-1 indicates N-H stretching of the secondary amine, the peak at

297   2241 cm-1 indicates C≡N stretching, the peak at 1519 cm-1 indicates N-H bending, the peak at

298   1068 cm-1 indicates C-O stretching, while the peak at 732 cm-1 indicates C=C bending. In the

299   FTIR spectra of TPP, the peak at 1127 cm^{-1} corresponds to the O–P=O stretching vibration, while

300   the peaks at 1211 cm^{-1} and 1097 cm^{-1} are associated with P=O and PO_3 stretching vibrations,

301   respectively, indicative of phosphorylated structures. Other significant peaks include 1116, 1087,

302   and 1028 cm^{-1} (C–O, C–C, and C–H vibrations), all of which are crucial in characterizing the

303   carbohydrate backbone. The infrared spectrum of cinnamon bark showed a sharp peak with high

304   intensity at 1662 cm-1, which indicates the stretching of the aldehyde carbonyl group C=O, which

305   represents a high concentration of aldehyde in CB. Also, the presence of significant peaks at the

306   range of 3630 to 2735 cm-1 indicated the stretching of alcohol O–H, the peak at 1134 cm-1

307   indicated the stretching of C–O, and finally the peak at 759 cm-1 indicated the bending of C=C.

308   The cross-linking of the chitosan polymer with TPP and CBE in the different concentrations of

309   nano extract CBE-CS resulted in a significant change in the peak groups at the peak 3329 cm-1

310   related to amide (N-H stretching of secondary amine) and the peak at 3379 cm-1 related to N-H

311   stretching of primary amine. It is also evident that the peak shape became distinctly sharp due to

312   the enhancement of hydrogen bonding, indicating the participation of TPP and amine groups in

313   chitosan in the chemical reaction. While the presence of new absorption peaks at 2870 cm-1

314   indicates O-H stretching and at 1624 cm-1 indicates C=C stretching, while the high intensity

315   stretching band at 1053 cm-1 indicates C-O stretching. In the nano-extract CBE-CS at 0% of TPP,

316   the distinct peaks at 1662 cm-1 indicated the extension of aldehyde carbonyl group by carbon =

317   oxygen) and the peak at 1134 cm-1 indicated the extension of aldehyde carbonyl group. The results

318   obtained in this study agree with the previous studies in references (Somenath Das et al., 2020),

319   (Prasad et al., 2022), (Deepika et al., 2021), (Deepika et al., 2021), and (Chaudhari et al., 2022).

320   **Fig 4: FTIR spectra of chitosan, TPP, CBE, CBE-CS at 0% TPP**

321

322   ## 3.5 Encapsulation efficiency (EE) and loading capacity (LC)

323   The EE and LC of CBE-CS nanocapsules were determined using UV-visible

324   spectrophotometry at the maximum absorption wavelength of CBE-CS. The results, illustrated in

325   Fig.5, demonstrate the impact of varying TPP concentrations on the LC and EE of the

326   nanocapsules. As the TPP concentration in the nanoemulsion increased, there was a notable

327   positive effect on the loading capacity of the nanocapsules. Specifically, the LC values rose from

328   25.65% to 33.9% as the TPP concentration increased from 0% to 4%. This trend indicates that

329   higher TPP concentrations enhance the ability of the nanocapsules to incorporate CBE. However,

330   if TPP is excessively increased, the nanoparticle structure might become too rigid and dense, which

331   could reduce the available space for drug loading, thereby decreasing the loading capacity. On the

332   other hand, the encapsulation efficiency remained relatively stable across all TPP concentrations,

333   with values ranging between 48.65% and 48.78%. The consistent EE suggests that a saturation

334   point may have been reached, beyond which further increases in TPP concentration do not

335   significantly impact encapsulation. These findings are consistent with previous studies. For

336   instance, (Culas et al., 2023), (Deepika et al., 2021), and (Amiri et al., 2021) also observed stable

337   encapsulation efficiencies in similar formulations. Conversely, studies by (Prasad et al., 2022), and

338   (Deepika et al., 2021) reported increases in both EE and LC with higher TPP concentrations.

339   **Fig.5: Effect of CBE loading at different TPP concentrations on encapsulation efficiency**

340   **and loading capacity (Value indicates mean of four replicates).**

341

342 3.6 In vitro release test

343   In vitro release kinetics test was performed where dried capsules were added in aqueous-

344   alcoholic medium at a volume ratio of 1:1. UV-visible spectroscopy at 286 nm wavelength was

345   used to evaluate the concentration of CBE (Ramasamy et al., 2017). Readings were taken at times

346   t = 0 (starting time), (t) 10, 20, 30, 60, 240, 1440, and 2880 min for triplicates. Fig.6 shows the

347   release of CB extract over time. As shown, after 1440 min, the release rate of CB extract was 0.44

348   μmol/mL. The curve is divided into two separate parts. The CBE concentration increases quickly

349 in the first section, which corresponds to the test's initial hours. In enclosed systems, this behavior

350 is frequently seen (Amiri et al., 2021). As the CB contained in the capsule core slowly reaches the

351 capsule surface, the second area of the curve shows a nearly constant CBE concentration, (Shetta

352 et al., 2019) and (Sibaja et al., 2015). Based on the concentration difference, these data show that

353 the CB release is connected to the concentration on the inside and external region of the capsule.

354 **Fig.6: The release kinetics of CB extract over time**

355

356 ## 3.7. Assessment of antibacterial activity, MIC, and MBC

357   Inhibition zone formation, MIC, and MBC are critical measures of antimicrobial effectiveness.

358 The in vitro evaluation of different CBE-CS nano-extract formulations against *B. glumae*

359 demonstrated varying degrees of antibacterial efficacy, as measured by the DIZ, the percentage of

360 inhibited radial growth (PIRG), and the increment of activity of the test discs. The results,

361 summarized in Table 3, reveal that all nano-formulations containing different concentrations of

362 TPP were effective, albeit to varying extents.

363 **Table 3: Disc diffusion method-based antimicrobial activities of CBE-CS nanobactericide**

364 **formulation and the antibiotic streptomycin against *B. glumae*.**

	CBE-CS formulation					DH2O	Pos. control
	0 % TPP	0.5 % TPP	1 % TPP	2% TPP	4% TPP		
Inhibition zone (mm)	8.6 ± 0.33^c	11.3 ± 0.33^b	11.5 ± 0.28^b	11.6 ± 0.76^b	11.3 ± 0.33^b	0.0 ± 0.0^d	20.0 ± 0.00^a

PIRG (%)	31.7	46.7	47.1	47.9	46.	-	-
Effectiveness Increase (%)	-	47.4	0.8	1.72	-2.5	-	-

365

366   The data indicates that the nano-extract with 0% TPP concentration exhibited the lowest

367 inhibition zone, measuring 7.8 mm. As TPP concentrations increased, a corresponding significant

368 increase in DIZ was observed, with values ranging from 11.5 to 11.8 mm for concentrations

369 between 0.5% and 2% (P>0.05). Notably, the nano-extract with 4% TPP concentration achieved a

370 DIZ of 15.5 mm, while the positive control treated with streptomycin resulted in the highest DIZ

371 at 24.6 mm, outperforming all other nano-pesticide formulations. Furthermore, the PIRG index

372 showed a positive correlation with increasing TPP concentrations, indicating enhanced

373 antibacterial activity. The most significant improvement in activity was observed at a TPP

374 concentration of 0.5%, with a remarkable increment of 47.4% in effectiveness. When determining

375 the MIC, the color change in the microtiter plate wells, which transitioned from colorless to bright

376 red, indicated the presence of live bacteria and the varying impact of TPP concentrations on

377 bacterial inhibition. The MIC value was determined to be 31.25 μmol/mL, while the MBC value

378 was 15.6 μmol/mL. These findings underscore the potent antibacterial activity of the CBE-CS

379 nano-extract against *B. glumae*, highlighting its potential as an effective antimicrobial agent.

380 ## 3.8. Time-killing analysis

381   The time-killing test was conducted to assess the bactericidal efficacy of CBE-CS 0.5% TPP

382 nano-extract at varying concentrations of MIC (0.5, 1, and 2) against *B. glumae*. A bacteria-free

383 control was used to establish a baseline, with its optical density (OD) remaining steady after an

384 initial increase during the first 18 hours of incubation. The results of the growth curve are

385 illustrated in Fig.7. The nano-extract demonstrated a concentration-dependent effect on the growth

386 rates of *B. glumae* throughout the 24-hour period. All tested concentrations of MIC showed a

387 reduction in bacterial growth rates within the first 4 hours. For concentrations of 0.5 MIC and 1

388 MIC, a slight decrease in the growth rate was observed after the initial 4-hour. In contrast, the

389 nano-extract at 2 MIC exhibited a more pronounced impact, with a significant decrease in the

390 growth curve observed after the first 4 hours until 8 hours. This result indicates that all MIC

391 concentration was highly effective, rapidly reducing the bacterial population and preventing

392 further growth.

393 **Fig.7: Time Killing analysis of the CBE-CS formulation against *B. glumae* at (0.5, 1, 2) of**

394 **MIC. The absorbance OD at 600 nm was measured until the 24 h.**

395

4. Conclusion

397 In this study, we developed a CBE-loaded nanoencapsulation aimed at controlling bacterial

398 panicle blight caused by *Burkholderia glumae* in rice plants. The nanoencapsulation was

399 formulated with varying concentrations of TPP (0%, 0.5%, 1%, 2%, and 4%) and characterized

400 for its internal structure, morphology, and size using TEM. The results revealed that all

401 nanoparticles were within the nanometer scale, with the introduction of TPP significantly

402 influencing their morphology. Specifically, TPP contributed to a more spherical shape, likely due

403 to the increased rigidity from cross-linking between TPP and chitosan (CS). Particle size analysis

404 during dissolution in deionized water showed an inverse relationship between TPP concentration

and nanoparticle size, with the smallest particles observed at 0.5% TPP. PDI analysis indicated a shift from monodisperse to polydisperse systems with higher TPP concentrations, suggesting decreased stability due to increased agglomeration. This instability may result from gel formation through inter- and intra-particle cross-linking. Zeta potential measurements revealed that increasing TPP concentrations caused a shift from positive to negative surface charges, attributed to the negatively charged functional groups of cinnamon molecules coating the nanoparticles. Higher zeta potential values indicate superior stability and functionality, while the observed negative zeta potentials may influence nanoparticle aggregation. FTIR analysis confirmed the successful encapsulation of CBE within the CS nanoparticles, as evidenced by characteristic absorption bands and peaks associated with both CBE and CS functional groups. The release of bioactive substances from the nanoparticles likely followed mechanisms such as disintegration, surface erosion, desorption, and diffusion. Initial rapid release within the first two hours, followed by a slower release, is crucial for effective bacterial control. The zone of inhibition tests confirmed the antibacterial efficacy of the CBE-CS nanobactericide against *B. glumae*, with a significant reduction in microbial count compared to the distilled water-negative control, where no inhibition was observed. This suggests that the CBE-CS formulation offers promising potential for managing BPB in rice plants.

Acknowledgment

Data Availability

427   Data will be available upon request.

References

429   Ağardan, N. B. M. (2020). Studies on the formulation optimization and controlled ionic gelation

430   of chitosan nanoparticles using TPP-HP-β-CD inclusion complex. *Istanbul Journal of*

431   *Pharmacy*, *50*(1), 54–59.

432   Alghuthaymi, M. A., Diab, A. M., Elzahy, A. F., Mazrou, K. E., Tayel, A. A., & Moussa, S. H.

433   (2021). Green biosynthesized selenium nanoparticles by cinnamon extract and their

434   antimicrobial activity and application as edible coatings with nano-chitosan. *Journal of*

435   *Food Quality*, *2021*(1), 6670709.

436   Amiri, A., Ramezanian, A., Mortazavi, S. M. H., Hosseini, S. M. H., & Yahia, E. (2021).

437   Shelf-life extension of pomegranate arils using chitosan nanoparticles loaded with Satureja

438   hortensis essential oil. *Journal of the Science of Food and Agriculture*, *101*(9), 3778–3786.

439   Anuranj, P. R., Harisankaran, P. S., Adithya, K. S., Parvathy, S., Prakash, G., Vishnu, S. V, Pran,

440   M., Chopra, H., Emran, T. Bin, & Dey, A. (2022). *Essential oils as valuable feed additive:*

441   *a narrative review of the state of knowledge about their beneficial health applications and*

442   *enhancement of production performances in poultry.*

443   Calvo, P., Remunan-Lopez, C., Vila-Jato, J. L., & Alonso, M. J. (1997). Novel hydrophilic

444   chitosan-polyethylene oxide nanoparticles as protein carriers. *Journal of Applied Polymer*

445   *Science*, *63*(1), 125–132.

446   Cava-Roda, R., Taboada-Rodríguez, A., López-Gómez, A., Martínez-Hernández, G. B., &

447   Marín-Iniesta, F. (2021). Synergistic antimicrobial activities of combinations of vanillin and

448   essential oils of cinnamon bark, cinnamon leaves, and cloves. *Foods*, *10*(6), 1406.

449   Chaudhari, A. K., Singh, V. K., Das, S., & Dubey, N. K. (2022). Fabrication, characterization,

450   and bioactivity assessment of chitosan nanoemulsion containing allspice essential oil to

451   mitigate Aspergillus flavus contamination and aflatoxin B1 production in maize. *Food*

452   *Chemistry*, *372*, 131221.

453   Chavez-Esquivel, G., Cervantes-Cuevas, H., Ybieta-Olvera, L. F., Briones, M. T. C., Acosta, D.,

454   & Cabello, J. (2021). Antimicrobial activity of graphite oxide doped with silver against

455   Bacillus subtilis, Candida albicans, Escherichia coli, and Staphylococcus aureus by agar

456   well diffusion test: Synthesis and characterization. *Materials Science and Engineering: C*,

457   *123*, 111934.

458   Chompa, S. S., Akter, A., Sadeq, A. B. M., Rahman, M. E., Rashid, H. O., Ibnat, N., & Hossain,

459   M. B. (2022). An overview of major bacterial diseases of rice and management strategies

460   for their control in Malaysia. *GSJ*, *10*(4).

461   Culas, M. S., Popovich, D. G., & Rashidinejad, A. (2023). Recent advances in encapsulation

462   techniques for cinnamon bioactive compounds: A review on stability, effectiveness, and

463   potential applications. *Food Bioscience*, 103470.

464   Deepika, Singh, A., Chaudhari, A. K., Das, S., & Dubey, N. K. (2021). Zingiber zerumbet L.

465   essential oil-based chitosan nanoemulsion as an efficient green preservative against fungi

466   and aflatoxin B1 contamination. *Journal of Food Science*, *86*(1), 149–160.

467   Deshi, V. V, Awati, M. G., Terdal, D., Patil, S. N., Ghandhe, A. R., Gudigennavar, A. S., Patalli,

468   P., Lata, D., Singh, D. R., & Siddiqui, M. W. (2024). Cinnamon essential oil incorporated

469   chitosan submicron emulsion as a sustainable alternative for extension of mango shelf life.

Sustainable Chemistry and Pharmacy, *41*, 101736.

Faizal Azizi, M. M., & Lau, H. Y. (2022). Advanced diagnostic approaches developed for the global menace of rice diseases: a review. *Canadian Journal of Plant Pathology*, *44*(5), 627–651.

Farooq, F., Hussain, Z., Hanief, M. I., & Fida, Z. (2023). CINNAMON (CINNAMOMUM ZEYLANICUM); A BRIEF REVIEW OF THE CULINARY SPICE WITH ITS POTENTIAL THERAPEUTIC INDICATIONS. *European Journal of Biomedical and Pharmaceutical Sciences*, *10*(6), 2349–8870.

Fernández-Díaz, C., Coste, O., & Malta, E. (2017). Polymer chitosan nanoparticles functionalized with Ulva ohnoi extracts boost in vitro ulvan immunostimulant effect in Solea senegalensis macrophages. *Algal Research*, *26*, 135–142.

Han, V.-C., Yu, N. H., Park, A. R., Yoon, H., Son, Y. K., Lee, B.-H., & Kim, J.-C. (2021). First report of shot-hole on flowering cherry caused by Burkholderia contaminans and Pseudomonas syringae pv. syringae. *Plant Disease*, *105*(12), 3795–3802.

Hasheminejad, N., Khodaiyan, F., & Safari, M. (2019). Improving the antifungal activity of clove essential oil encapsulated by chitosan nanoparticles. *Food Chemistry*, *275*, 113–122.

Hoang, N. H., Le Thanh, T., Sangpueak, R., Treekoon, J., Saengchan, C., Thepbandit, W., Papathoti, N. K., Kamkaew, A., & Buensanteai, N. (2022). Chitosan nanoparticles-based ionic gelation method: a promising candidate for plant disease management. *Polymers*, *14*(4), 662.

Huang, K.-S., Sheu, Y.-R., & Chao, I.-C. (2009). Preparation and properties of nanochitosan.

Polymer-Plastics Technology and Engineering, *48*(12), 1239–1243.

Kaboudi, Z., Peighambardoust, S. H., Nourbakhsh, H., & Soltanzadeh, M. (2023). Nanoencapsulation of Chavir (Ferulago angulata) essential oil in chitosan carrier: Investigating physicochemical, morphological, thermal, antimicrobial and release profile of obtained nanoparticles. *International Journal of Biological Macromolecules*, *237*, 123963.

Koul, B., Poonia, A. K., Yadav, D., & Jin, J. O. (2021). *Microbe-Mediated Biosynthesis of Nanoparticles: Applications and Future Prospects. Biomolecules 2021, 11, 886*. s Note: MDPI stays neutral with regard to jurisdictional claims in published ….

Kumar, M., Kumar, A., Shukla, P., Mishra, A. K., & Kumar, A. (2023). Biology of Rice Bacterial Brown Stripe Pathogen and Integrated Strategies for Its Management. *Journal of Experimental Agriculture International*, *45*(1), 1–8.

Lunardi, C. N., Gomes, A. J., Rocha, F. S., De Tommaso, J., & Patience, G. S. (2021). Experimental methods in chemical engineering: Zeta potential. *The Canadian Journal of Chemical Engineering*, *99*(3), 627–639.

Maluin, F. N., Hussein, M. Z., Yusof, N. A., Fakurazi, S., Idris, A. S., Hilmi, N. H. Z., & Jeffery Daim, L. D. (2019). A potent antifungal agent for basal stem rot disease treatment in oil palms based on chitosan-dazomet nanoparticles. *International Journal of Molecular Sciences*, *20*(9), 2247.

Mini Raj, N., Vikram, H. C., Muhammed Nissar, V. A., & Nybe, E. V. (2023). Cinnamon and Indian Cinnamon (Indian Cassia). In *Handbook of Spices in India: 75 Years of Research and Development* (pp. 2921–2991). Springer.

Mujtaba, M., Khawar, K. M., Camara, M. C., Carvalho, L. B., Fraceto, L. F., Morsi, R. E.,
Elsabee, M. Z., Kaya, M., Labidi, J., & Ullah, H. (2020). Chitosan-based delivery systems
for plants: A brief overview of recent advances and future directions. *International Journal
of Biological Macromolecules*, *154*, 683–697.

Pathak, R., Bhatt, S., Punetha, V. D., & Punetha, M. (2023). Chitosan nanoparticles and based
composites as a biocompatible vehicle for drug delivery: a review. *International Journal of
Biological Macromolecules*, 127369.

Prasad, J., Das, S., Maurya, A., Jain, S. K., & Dwivedy, A. K. (2022). Synthesis, characterization
and in situ bioefficacy evaluation of Cymbopogon nardus essential oil impregnated chitosan
nanoemulsion against fungal infestation and aflatoxin B1 contamination in food system.
International Journal of Biological Macromolecules, *205*, 240–252.

Rahman, A., Jahuddin, R., Bahar, A. K. F., Yani, A., & Patandjengi, B. (2024). Detection of the
presence of bacteria causing grain rot disease (Burkholderia glumae) in some rice seed
producers in South Sulawesi, Indonesia. *Jurnal Hama Dan Penyakit Tumbuhan Tropika*,
24(1), 10–16.

Ramachandran, K., Vijaya, S. I., Ahmad, F. N., Amzah, B., & Zakaria, L. (2021).
Characterization and identification of Burkholderia glumae as the causal pathogen of
bacterial panicle blight of rice (Oryza sativa L.) in Malaysian rice granaries. *Journal of
General Plant Pathology*, *87*, 164–169.

Ramasamy, M., Lee, J.-H., & Lee, J. (2017). Direct one-pot synthesis of cinnamaldehyde
immobilized on gold nanoparticles and their antibiofilm properties. *Colloids and Surfaces
B: Biointerfaces*, *160*, 639–648.

534 Rashid, M. R., Zaidi, A. B. M., Noriha, M. A., Sabrina, W. N., Hazalina, Z., & Noor Azlina, M.

535   (2022). *Preliminary screening of antagonistic rice-associated rhizobacteria on*

536   *Burkholderia glumae.*

537 Sharifi-Rad, J., Dey, A., Koirala, N., Shaheen, S., El Omari, N., Salehi, B., Goloshvili, T., Cirone

538   Silva, N. C., Bouyahya, A., & Vitalini, S. (2021). Cinnamomum species: bridging

539   phytochemistry knowledge, pharmacological properties and toxicological safety for health

540   benefits. *Frontiers in Pharmacology*, *12*, 600139.

541 Shetta, A., Kegere, J., & Mamdouh, W. (2019). Comparative study of encapsulated peppermint

542   and green tea essential oils in chitosan nanoparticles: Encapsulation, thermal stability, in-

543   vitro release, antioxidant and antibacterial activities. *International Journal of Biological*

544   *Macromolecules*, *126*, 731–742.

545 Sibaja, B., Culbertson, E., Marshall, P., Boy, R., Broughton, R. M., Solano, A. A., Esquivel, M.,

546   Parker, J., De La Fuente, L., & Auad, M. L. (2015). Preparation of alginate–chitosan fibers

547   with potential biomedical applications. *Carbohydrate Polymers*, *134*, 598–608.

548 Somenath Das, S. Das, Singh, V. K., Dwivedy, A. K., Chaudhari, A. K., Neha Upadhyay, N. U.,

549   Akanksha Singh, A. S., Deepika, D., & Dubey, N. K. (2020). *Fabrication, characterization*

550   *and practical efficacy of Myristica fragrans essential oil nanoemulsion delivery system*

551   *against postharvest biodeterioration.*

552 Ul-Islam, M., Alabbosh, K. F., Manan, S., Khan, S., Ahmad, F., & Ullah, M. W. (2024).

553   Chitosan-based nanostructured biomaterials: Synthesis, properties, and biomedical

554   applications. *Advanced Industrial and Engineering Polymer Research*, *7*(1), 79–99.
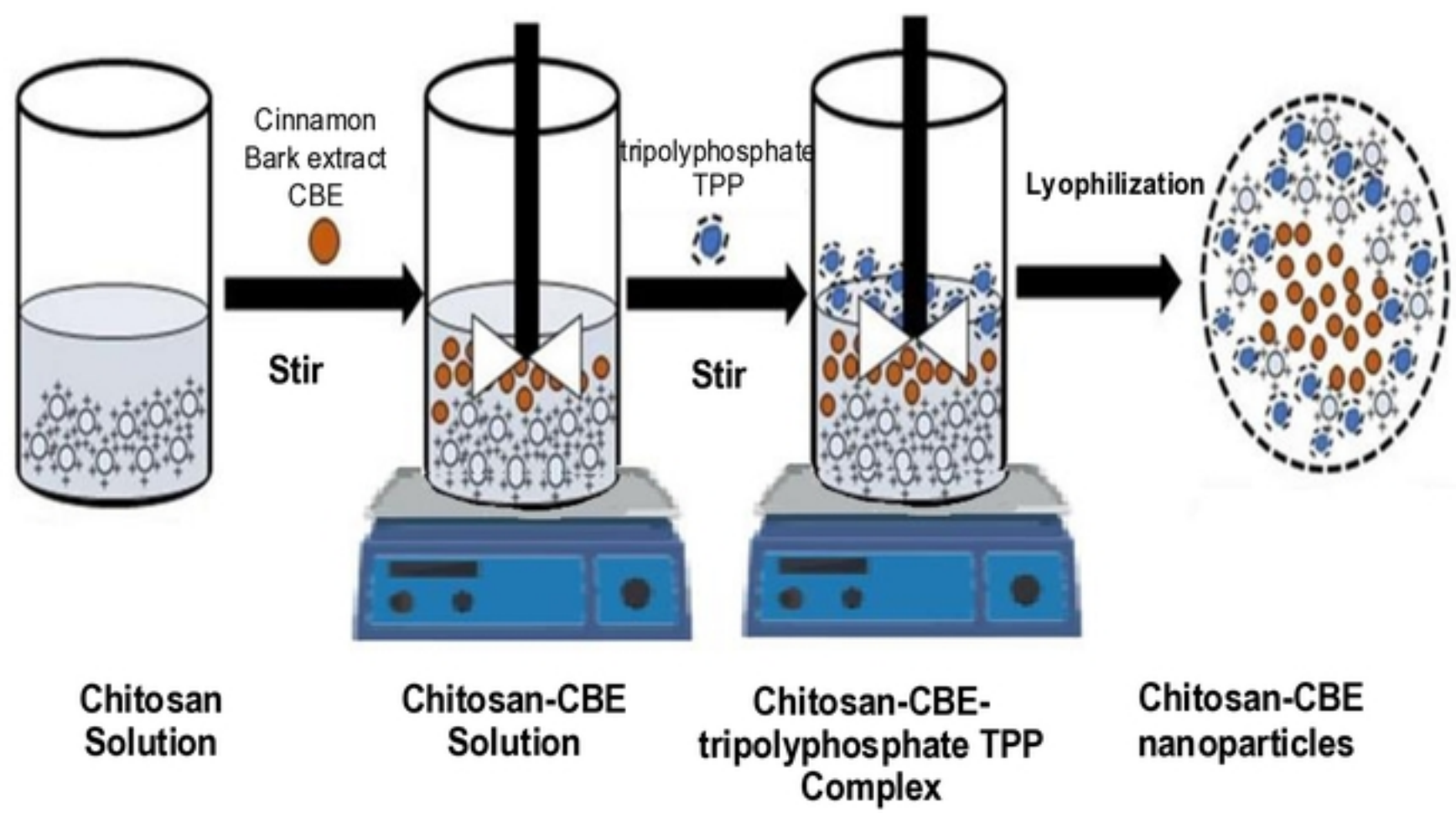
555 Veerasingam, S., Ranjani, M., Venkatachalapathy, R., Bagaev, A., Mukhanov, V., Litvinyuk, D.,

556   Mugilarasan, M., Gurumoorthi, K., Guganathan, L., & Aboobacker, V. M. (2021).

557   Contributions of Fourier transform infrared spectroscopy in microplastic pollution research:

558   A review. *Critical Reviews in Environmental Science and Technology*, *51*(22), 2681–2743.
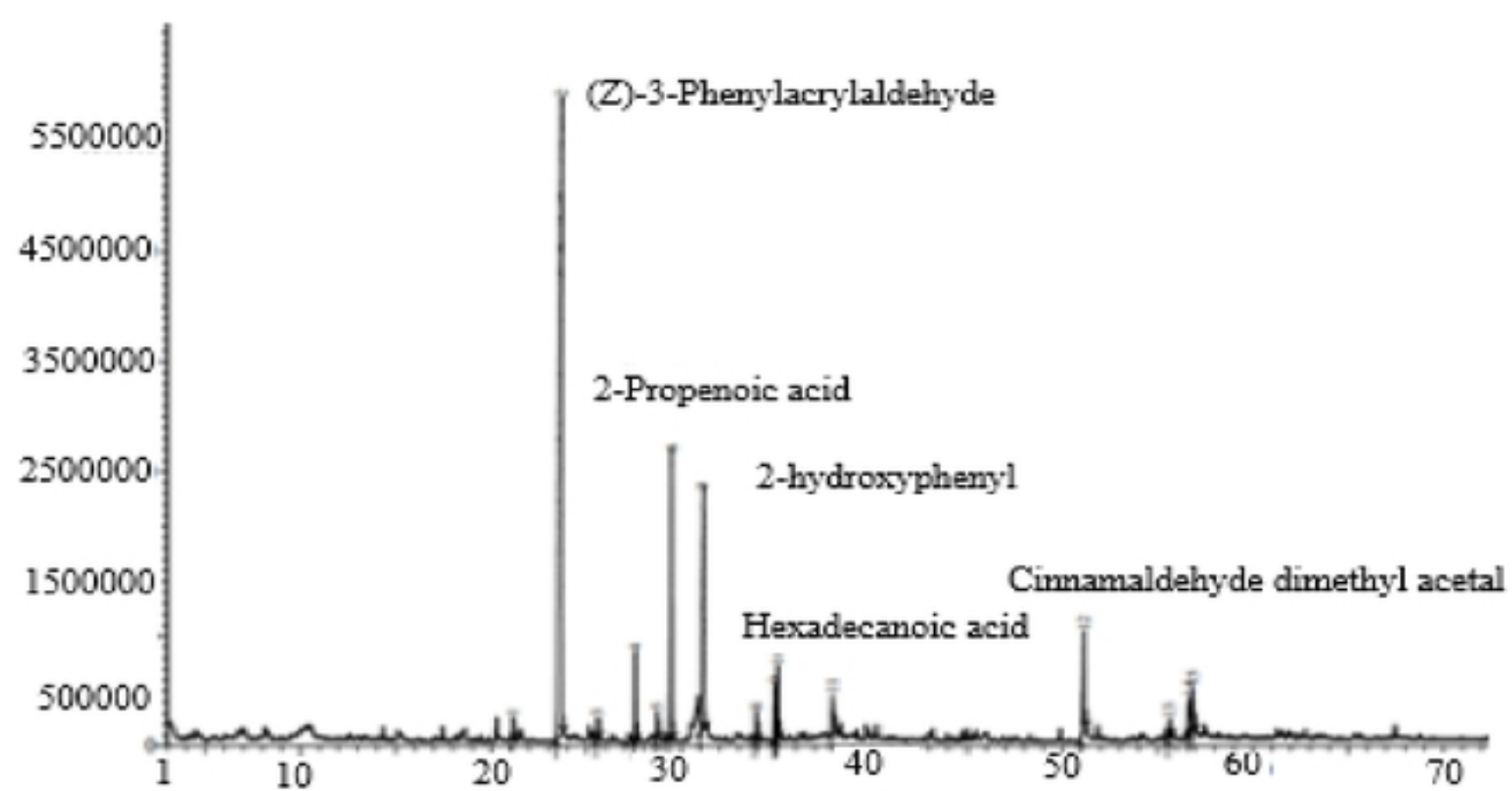
559 Verma, D. K., & Srivastav, P. P. (2020). Bioactive compounds of rice (Oryza sativa L.): Review

560   on paradigm and its potential benefit in human health. *Trends in Food Science &*

561   *Technology*, *97*, 355–365.

562 Wang, Y., Zhao, J., Xu, F., Wu, X., Hu, W., Chang, Y., Zhang, L., Chen, J., & Liu, C. (2020).

563   GC-MS, GC-O and OAV analyses of key aroma compounds in Jiaozi Steamed Bread.

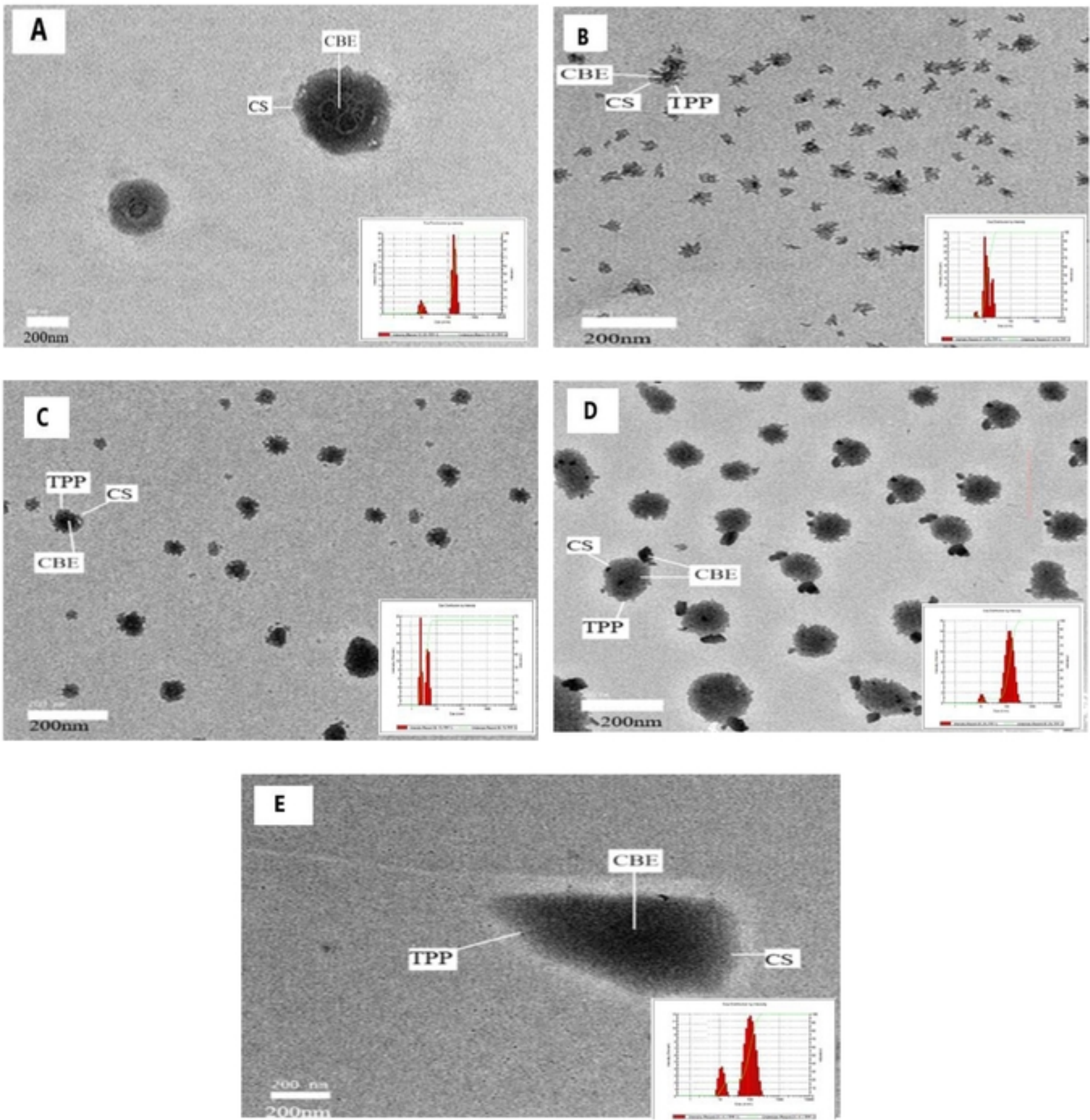564   *Grain & Oil Science and Technology*, *3*(1), 9–17.

565 Zhang, J., Zhu, Y., Yu, L., Yang, M., Zou, X., Yin, C., & Lin, Y. (2022). Research advances in

566   cadmium uptake, transport and resistance in rice (Oryza sativa L.). *Cells*, *11*(3), 569.

567

568

569

570

571

572

573

574

575

576

577

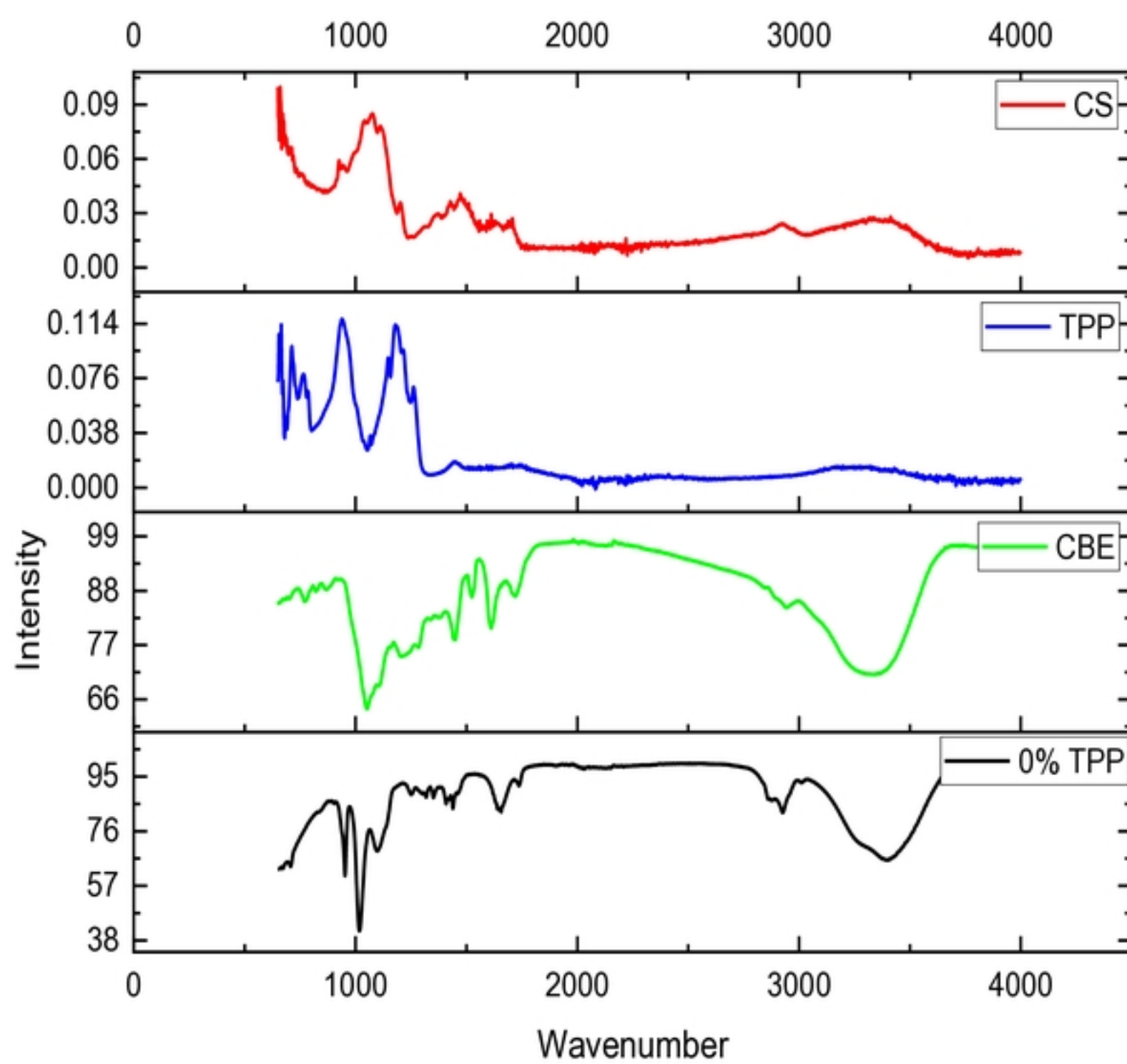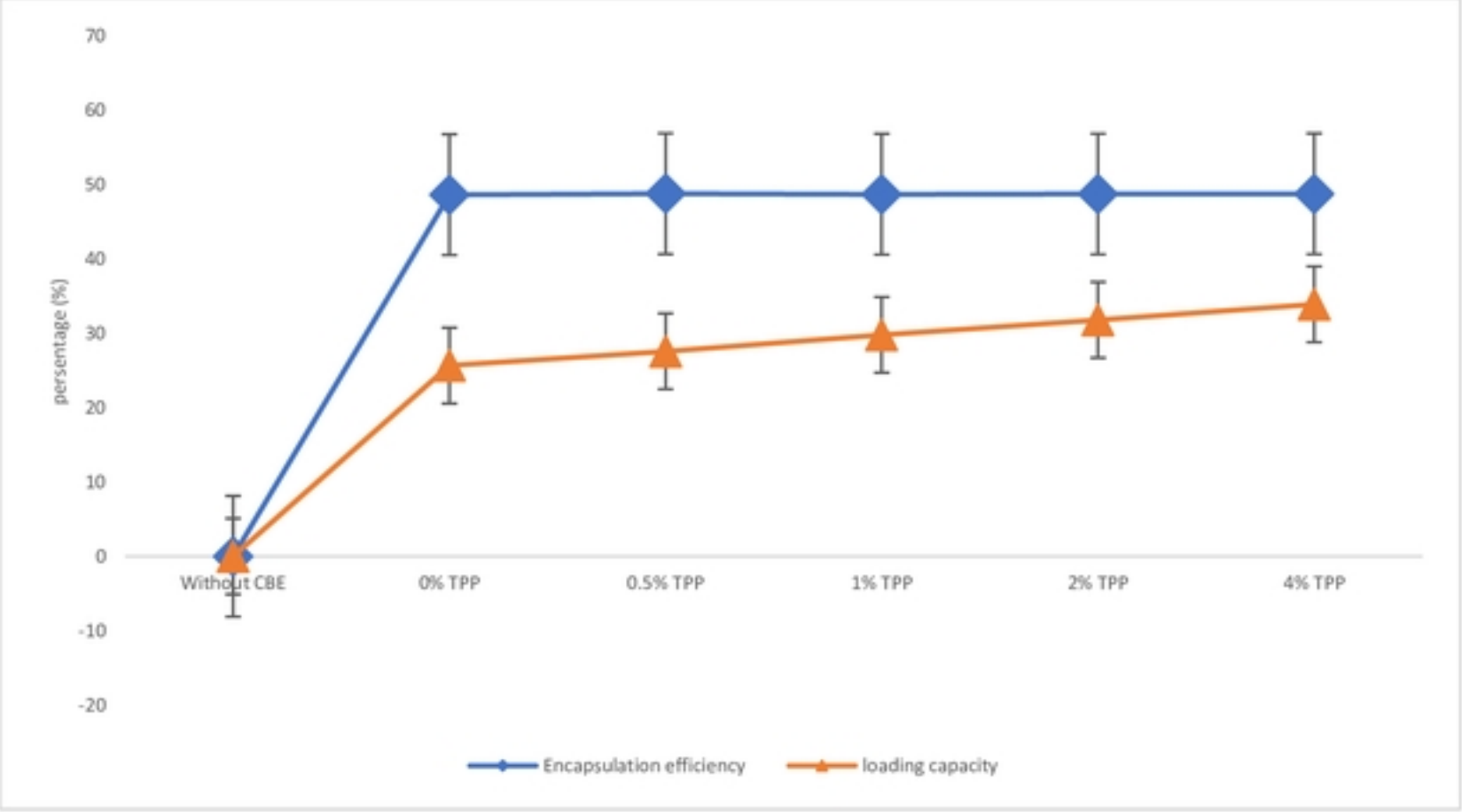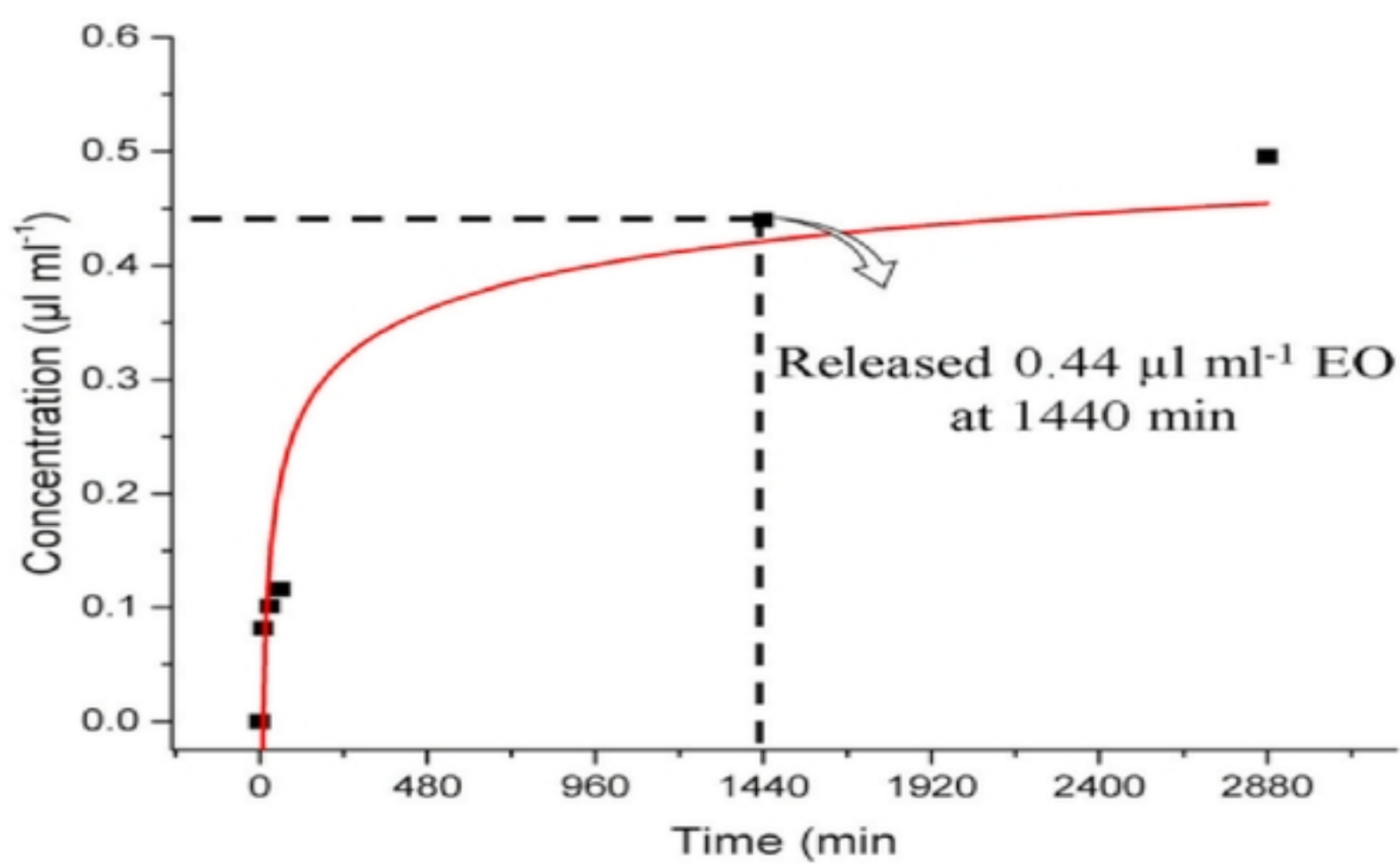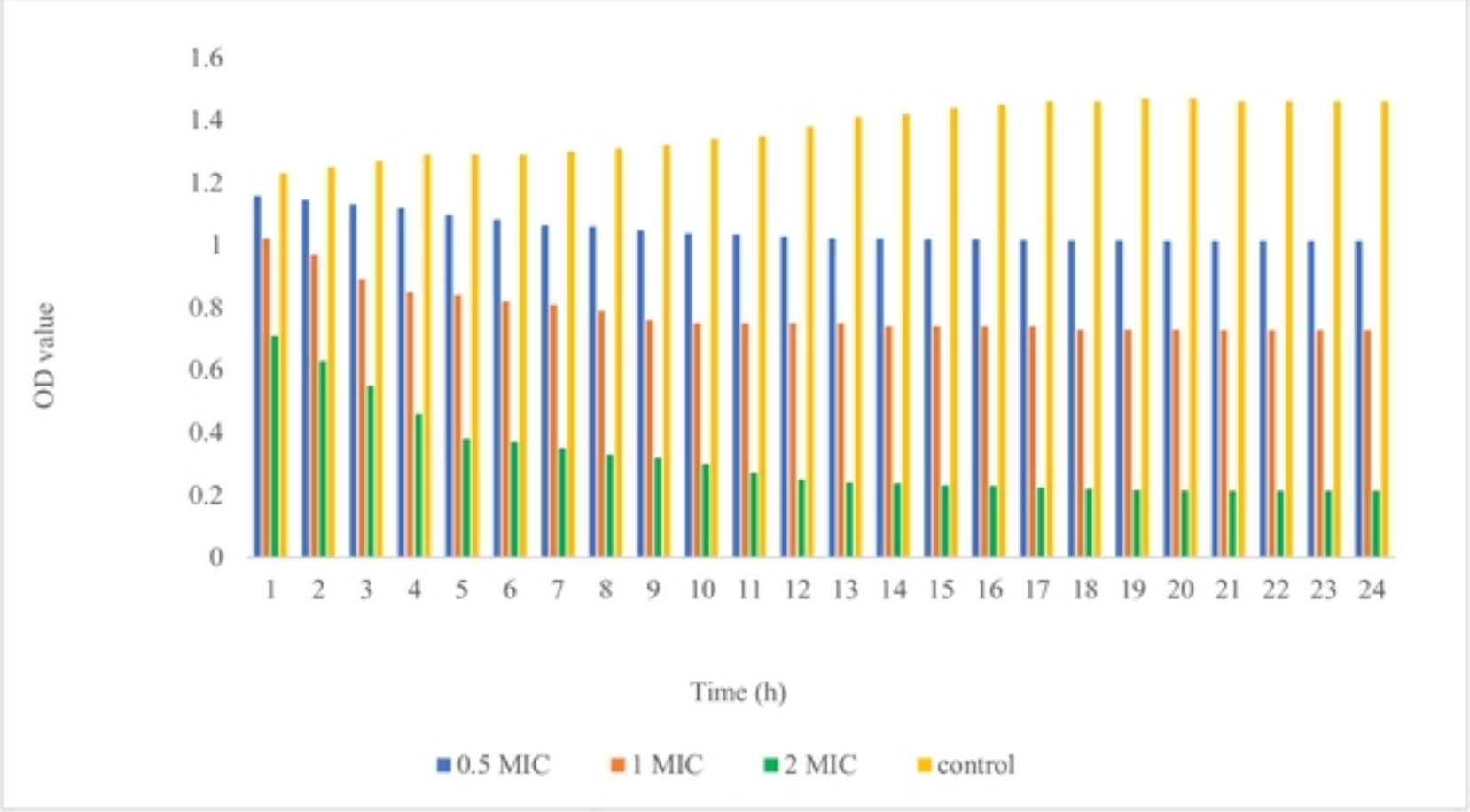| Chitosan Solution | Chitosan-CBE Solution | Chitosan-CBE-tripolyphosphate TPP Complex | Chitosan-CBE nanoparticles |

Figure

Figure

Figure

Figure

Figure

Figure

Figure